

Stimulated Compton scattering by a relativistic electron beam

P. G. Zhukov, V. S. Ivanov, M. S. Rabinovich, M. D. Raizer, and A. A. Rukhadze

P. N. Lebedev Physics Institute, USSR Academy of Sciences

(Submitted 6 December 1978)

Zh. Eksp. Teor. Fiz. 76, 2065–2074 (June 1979)

We describe experiments on the Compton scattering of electromagnetic waves in a circular metallic waveguide by a relativistic electron beam. We discuss the features of the Compton scattering in a waveguide, and in particular, we analyze the dependence of the frequencies of the scattered radiation on the parameters of the system and on the frequency of the incident radiation. We indicate the conditions for neglect of the thermal spread of the electron beam. From comparison of theoretical ideas and experimental results regarding the dependence of the power of the radiation scattered at various frequencies on the power of the incident wave, we conclude that the observed scattering is stimulated. We determine the experimental conditions under which partial reflection of the radiation from the ends of the system becomes important and the stimulated-scattering process goes over to one of generation.

PACS numbers: 41.90. + e, 84.40.Ts

§ 1. GENERAL RELATIONS

As a result of the development of pulsed relativistic high-current electrons the observation of the phenomenon of stimulated Compton scattering predicted by Kapitsa and Dirac¹ has become a reality. This phenomenon opens the possibility of conversion of long-wavelength electromagnetic radiation into short-wavelength radiation and therefore has produced significant interest in recent years.²⁻⁵ The first experiments on observation of short-wavelength radiation in Compton scattering of centimeter microwaves by a relativistic electron beam have already been carried out,² and the possibility is being seriously discussed of constructing Compton amplifiers and generators of millimeter radiation.⁵

In the present work we describe experiments on stimulated Compton scattering of an intense pulse of electromagnetic waves of the centimeter region by a high-current electron beam, carried out in the Terek-1 installation.⁶ Before turning to description of these experiments and their discussion, we present some general relations which characterize the scattering of electromagnetic waves in a waveguide.

Stimulated Compton scattering by an electron beam consists of the breakup (transition) of the incident electromagnetic wave into a scattered wave and density oscillations of the electrons (a longitudinal wave in the beam). The conditions for realization of such breakup in the beam coordinate system are written in the form

$$\omega_1' = \omega_2' + \omega_0, \quad \mathbf{k}_1' = \mathbf{k}_2' + \mathbf{k}_0. \quad (1.1)$$

Here ω_1' , \mathbf{k}_1' , and ω_2' , \mathbf{k}_2' —respectively the frequencies and wave vectors of the incident and scattered waves in the beam system, are related to ω_1 , \mathbf{k}_1 and ω_2 , \mathbf{k}_2 in the laboratory system by the equations of the Lorentz transformation (see the Appendix), and ω_0 and \mathbf{k}_0 are the frequency and wave vector of the longitudinal oscillations in the beam in the moving system.

Under conditions when ω_1' and ω_2' are much greater than the Larmor frequency of rotation of the electrons in a longitudinal magnetic field H_0 , i. e., $(\omega_1', \omega_2') \gg \omega_H = eH_0/mc$, we obtain from simple kinematic considera-

tions and the conditions for the breakup (1.1) ($\alpha = 1, 2$)

$$\frac{\omega_2}{\omega_1} = \gamma^2 \left(1 + \beta \cos \varphi_1 - \frac{\omega_0}{\gamma \omega_1} \right) \times \left\{ 1 \pm \beta \left[1 - \frac{\omega_{k_2}^2 + \omega_0^2}{\gamma^2 \omega_1^2 (1 + \beta \cos \varphi_1 - \omega_0/\gamma \omega_1)^2} \right]^{1/2} \right\}, \quad (1.2)$$

$$\cos \varphi_\alpha = \pm \left[1 - \frac{\omega_{k_\alpha}^2 + \omega_0^2}{\omega_\alpha^2} \right]^{1/2}.$$

Here $\omega_{k_\alpha} = c\mu_{\alpha i s}/R$ is the invariant critical frequency for the mode with radial wave number μ [for E waves we have $J_0(\mu_{1s}) = 0$ and for H waves we have $J_0'(\mu_{1s}) = 0$] in a waveguide with radius R , $\omega_b = (4\pi e^2 n_0/m\gamma)^{1/2}$ is the Langmuir frequency of an electron beam with density n_0 in the laboratory system, $\gamma = (1 - \beta^2)^{-1/2}$ is the relativistic factor of the electron energy, and the angles φ_α characterize the directions of propagation of the waves: For the incident wave $\cos \varphi_1 < 0$, for the scattered wave $\cos \varphi_2 < 0$ if the scattering occurs forward, and $\cos \varphi_2 > 0$ if backward scattering occurs, and in magnitude we have $|\cos \varphi_\alpha| = \beta_{\text{ifm } \alpha} = v_{\text{ifm } \alpha}/c$, i. e., this quantity determines the group velocities of the incident and scattered waves.

The two signs in Eq. (1.2) indicate that each radial mode of the scattered wave corresponds to two frequencies. This is evident from Fig. 1, where we have plotted the ratio ω_1/ω_2 as a function of μ_{2is} (the solid and dot-dash lines) and the ratio ω_2/ω_1 as a function of μ_{2is} (the dashed line) for a given mode of the incident wave $\mu_{01} = 2.4$ (the mode E_{01}) and the following system parameters: $R = 1.5$ cm, $\gamma = 2.4$, $\omega_1 = 6 \times 10^{10}$ sec⁻¹, $\omega_b = \omega_0 = 3 \times 10^{10}$ sec⁻¹.¹⁾ It is evident that only those radial modes μ_{2is} are allowed which satisfy the condition of reality of the ratio (1.2), which also determines the maximum value of μ_{2is} in Fig. 1, which is 10. In addition, propagation of modes with $|\cos \varphi_2| \approx 0$ is hindered in the waveguide (in pulsed systems they cannot be formed). In Fig. 1 (dashed line) this region corresponds to $\mu_{2is} = 4-6$.

Let us turn now to the dynamical relations and give the spatial amplification coefficient (gain) of the scattered electromagnetic wave in stimulated Compton scattering. According to Ref. 8 the time increment of the growth of the breakup process of interest to us in the

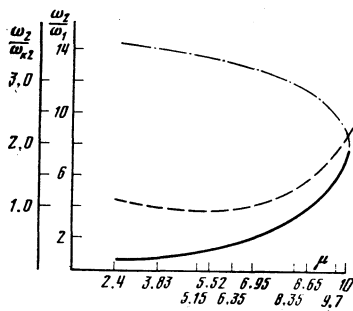


FIG. 1.

beam coordinate system is determined from the dispersion equation

$$1 + \delta e'(\omega_0, k_0) + \frac{k_0^2 \delta e'(\omega_0, k_0) \omega_2'^2 [k_x' v_{E1}']^2}{4 \omega_1'^2 k_2'^2 (\omega_2'^2 - \omega_0^2 - c^2 k_x'^2)} = 0. \quad (1.3)$$

Here $v_{E1}' = eE_1'/m\omega_1'$ is the velocity of the oscillations of the electrons in the field of the incident wave and $\delta e'(\omega_0, k_0) + 1$ is the longitudinal permittivity of the electron plasma (beam), the zeros of which determine the spectrum of longitudinal waves ω_0 . In solution of Eq. (1.3) it is necessary to take into account that the time increment of growth is $\delta' = \text{Im}\omega_0 = -\text{Im}\omega_2'$.

As a result we find for the case of a monoenergetic beam

$$\delta' = \frac{1}{4} \left(\frac{[k_x' v_{E1}']^2}{\omega_1'^2} \frac{k_0^2}{k_2'^2} \omega_0 \omega_2' \frac{k_{0x}}{k_0} \right)^{1/2};$$

$$\text{Re } \omega_0 = \omega_b \frac{k_{0x}}{k_0} \gg \delta',$$

$$\delta' = \frac{\sqrt{3}}{2} \left(\frac{[k_x' v_{E1}']^2}{8 \omega_1'^2} \frac{k_0^2}{k_2'^2} \omega_0 \omega_2' \right)^{1/2};$$

$$\text{Re } \omega_0 \frac{1}{\sqrt{3}} \delta' \gg \omega_b \frac{k_{0x}}{k_0}. \quad (1.4)$$

The first of these increments corresponds to resonance Raman scattering, or breakup, and the second to modified breakup. It is therefore not astonishing that in the limit $\beta \rightarrow 0$ the expressions (1.4) go over to those obtained by Andreev⁹ for the growth increments of breakup instabilities.

The quantity δ' , like the remaining quantities in Eq. (1.4), is written in the beam system. It is not difficult to write these quantities in the laboratory system. In view of their cumbersome nature they are given in the Appendix. Here we have calculated only the spatial amplification coefficient for the power of the scattered radiation in the laboratory system:

$$\Gamma = \frac{2}{(\beta + \beta_{\text{lim}2}) c \gamma} \delta'. \quad (1.5)$$

Finally we note that according to Eq. (1.4) at high intensities of the incident radiation the scattering has the nature of a modified breakup, and at relatively low intensities it has the nature of resonance (Raman) breakup. However, even in this latter case the field of the incident wave must be sufficiently strong that dissipative processes due to the thermal spread of the electrons can be neglected. This requirement reduces to the following inequalities:

$$1 \gg \frac{\delta' k_0}{\omega_b k_{0x}} \gg \sqrt{\frac{\pi}{8}} \frac{1}{\xi^3} \exp\left(-\frac{1}{2\xi^2}\right),$$

$$\xi = \frac{k_0 c \Delta \varepsilon \gamma - 1}{\omega_b \varepsilon 2\gamma} \ll 1, \quad (1.6)$$

where $\Delta \varepsilon$ is the energy spread of the electrons in the laboratory coordinate system and $\varepsilon = mc^2(\gamma - 1)$ is the kinetic energy of the electrons. If these inequalities are not satisfied in the limit of low intensities of the incident radiation, the thermal spread of the electrons of the beam turns out to be dominant and the breakup instability acquires a kinetic nature with an exponentially small increment. We shall not, however, dwell on this case, which is of little interest.

§ 2. THE EXPERIMENT AND ITS RESULTS

The basic scheme of the experiment is shown in Fig. 2. As electron injector we used the high-current accelerator Terek-1,⁶ in which the electron flow is produced by a gun with magnetic insulation 1. The cathode of the gun was a hollow cylinder of graphite with outer diameter 20 mm and internal diameter 18 mm; the anode was a cylinder of stainless steel of diameter 40 mm. The gun was placed in a uniform quasistationary magnetic field which was produced by a pulsed solenoid 5. A magnetic field strength $B_0 = 0.4$ teslas provided magnetic insulation of the cathode assembly and transport of the electron flux 2 through the interaction space—the circular waveguide 3 and carcinotron 4. The diameters of the electron stream were determined from the track on a copper foil; the outer diameter was 21 mm, and the inner diameter 17 mm. The total beam current was measured by low-inductance shunts 6 and 7 with accuracy to $\pm 5\%$ and in the interaction space amounted to $I_b = 4.2$ kA. The electron energy was measured by a capacitance divider (accuracy of measurement $\pm 10\%$) and amounted to 670 ± 70 keV. The length of the current pulse at half-height was ~ 20 nsec. The residual gas pressure in the system did not exceed 2×10^{-5} Torr.

The carcinotron 4 is similar to that described previously.¹⁰ The working mode of the generated wave was E_{01} , the wavelength 3.2 mm, and the radiation pulse length at half-height ~ 15 nsec. The generator load is the horn 11 radiating into free space. The electromagnetic wave excited by the electron stream in the carcinotron propagates in the direction opposite to the electron flow in the interaction space 3—a circular waveguide of length 60 cm and radius 1.5 cm—and is reflected from the restriction 8 which is beyond cutoff for the mode E_{01} . After reflection the wave, practically without interacting with the electron stream, passes through the interaction space, the carcinotron, the circular waveguide with the bend 9, a mica vacuum window 10, and is radiated into free space from the horn 11.

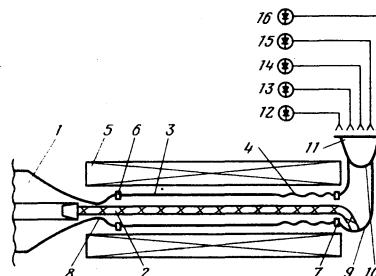


FIG. 2.

The system of measurement of the high-frequency power P_1 , as in Ref. 10, consisted of a receiving horn 12 connected by a single-mode waveguide with a cryogenically cooled semiconductor detector.¹¹ The sensitivity of the detector, the coefficient of radiation transfer from horn to horn, and the loss in the measuring circuit were determined by a special calibration setup.

The scattered electromagnetic radiation excited in the interaction space also passes through the carcinotron and is radiated into free space by means of the horn 11. The system of measurement of the power of the scattered radiation consisted of receiving horns 13–16 connected by single-mode waveguides with cryogenically cooled semiconductor detectors. The frequency of the radiation was measured by means of a system of waveguides beyond cutoff, located in front of the detectors. As can be seen from Fig. 1, in the system investigated it is necessary to expect scattered radiation at frequencies $\omega_2 = 2.5\omega_1$ ($\lambda_2 = 13.2$ mm, mode E_{31}), $\omega_2 = 2.6\omega_1$ ($\lambda_2 = 12.2$ mm, mode E_{12}), $\omega_2 = 3.8\omega_1$ ($\lambda_1 = 8.4$ mm, mode E_{22}), $\omega_2 = 4.3\omega_1$ ($\lambda_2 = 7.7$ mm, mode E_{08}), $\omega_2 = 6.1\omega_1$ ($\lambda_2 = 5.4$ mm, mode E_{32}), and $\omega_2 = (11-15)\omega_1$ (the set of modes with $\lambda_2 \leq 3.2$ mm). Therefore we used a system of waveguides beyond cutoff which permitted the scattered radiation to be recorded in four ranges of the wavelength λ_2 : 13.4 ± 1 , 7.8 ± 0.5 , 4.75 ± 1.5 , and ≤ 3.2 mm. The lower threshold of sensitivity of the entire measuring apparatus in each wavelength range was respectively 500, 500, 100, and 10 watts.

In the experiment we measured the scattered-radiation power P_2 in the indicated wavelength ranges as a function of the incident pumping-wave power P_1 . Here the power of the pumping wave was varied over a wide range, $P_1 = 10-300$ MW, for a constant electron beam current $I_b = 4.2$ kA in the interaction space. This was achieved by means of small angular shifts of the carcinotron axis with respect to the beam axis in the interaction space—here a part of the electron stream was lost at the entrance to the carcinotron.

The results of the measurements are shown in Fig. 3. In Fig. 3a we have plotted the clearly nonlinear dependence of the power P_2 of the scattered radiation on the power P_1 of the incident wave in the range $\lambda_2 = 13.4 \pm 1$ mm. It is evident that in the region $P_1 = 10-60$ MW we have a ratio $P_2/P_1 \approx 6 \times 10^{-4}$, while in the region $P_1 = 60-90$ MW this ratio rises significantly and $P_2/P_1 \approx 4 \times 10^{-3}$. The maximum value of the scattered-radiation power $P_2 \approx 140$ kW in this region is achieved for $P_1 \approx 100$ MW. Beginning with $P_1 \geq 100$ MW, an appreciable radiation appeared in the wavelength region $\lambda_2 = 7.8 \pm 0.5$ mm, which makes it difficult to measure accurately the scattered radiation at wavelength $\lambda_2 = 13.4 \pm 1$ mm. Therefore, beginning with a power $P_1 \geq 100$ MW, no measurements of the scattered-radiation power were made at this wavelength.

The dependence of P_2 on P_1 at a wavelength $\lambda_2 = 7.8 \pm 0.5$ mm is shown in Fig. 3, from which it can be seen that the maximum power of the scattered radiation in this region reaches $P_2 \approx 65$ kW for a ratio $P_2/P_1 \approx 6 \times 10^{-4}$.

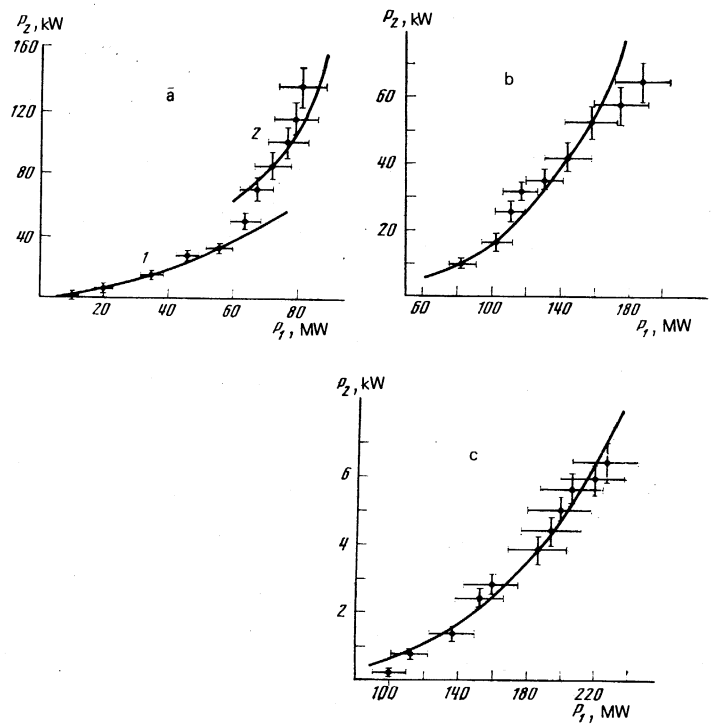


FIG. 3. Scattered-radiation power as a function of pumping-wave power. a— $\lambda = 13.4 \pm 1$ mm, curve 1— $P_0 = 1000$ W, curve 2— $P_0 = 1800$ W; b— $\lambda = 7.8 \pm 0.5$ mm, $P_0 = 170$ W; c— $\lambda = 4.75 \pm 1.5$ mm, $P_0 = 7.1$ W. ●—experimental data; solid line—calculation with the formula $P_2 = P_0 \exp(4.6 \times 10^{-4} P_1^{1/2})$.

For $P_1 \geq 180$ MW, appreciable radiation appears in the wavelength region $\lambda_2 = 4.75 \pm 1.5$ mm, and therefore measurements of the scattered radiation at wavelength $\lambda_2 = 7.8 \pm 0.5$ mm were discontinued.

In Fig. 3c we have shown measurements of P_2 as a function of P_1 in the region $P_1 \geq 180$ MW at a scattered-radiation wavelength $\lambda_2 = 4.75 \pm 1.5$ mm. In this wavelength range the maximum power is $P_2 \approx 6.5$ kW with $P_2/P_1 \approx 5 \times 10^{-5}$.

Finally, appreciable radiation in the wavelength range $\lambda_2 \leq 3.2$ mm was recorded only with $P_1 \approx 300$ MW, where $P_2 \approx 20$ W and the power ratio was $P_2/P_1 \approx 10^{-7}$.

We note the following principal features of the scattered radiation detected.

1. In all scattered-radiation wavelength regions investigated the dependence of P_2 on P_1 is very strong: for a change in power of the pumping wave by less than a factor two the power of the scattered radiation changes by almost an order of magnitude. In the wavelength region $\lambda_2 = 13.4 \pm 1$ mm this dependence is clearly nonlinear in nature (Fig. 3a).

TABLE I.

λ_2 , mm	P_1 , MW	P_2/P_1	P_{\min} , W	α , W ^{-1/2}	$e \Gamma L$	P_0 , W
13.4±1.0	10	4·10 ⁻³	500	2.4·10 ⁻⁴	14-60	1000; 1800
7.8±0.5	70	5·10 ⁻⁴	500	1.4·10 ⁻⁴	100-500	170
4.75±1.5	120	3·10 ⁻⁵	100	1.6·10 ⁻⁴	200-1000	7.1
≈3.2		7·10 ⁻⁸	10	4.4·10 ⁻⁴	3000	

2. With decrease of the scattered-radiation wavelength the pumping-wave power P_1^* at which P_2 reaches a definite level increases. Data for $P_2 = 1$ kW are given in the table.

3. With decrease of the scattered-radiation wavelength the ratio P_2/P_1 decreases (see Table I).

§ 3. DISCUSSION AND CONCLUSIONS

Under the conditions of the experiment $n_0 \approx 8 \times 10^{11}$ cm⁻³, $\omega_b \approx 3 \times 10^{10}$ sec⁻¹, $B_0 = 0.4$ T, and $\omega_H = 7 \times 10^{10}$ sec⁻¹, which assured satisfaction of the inequality $\omega_H^2 > \omega_b^2$ but $\omega_1' = \omega_1 \gamma (1 + \beta \beta_{11m1}) \approx \omega_2' \approx 22 \times 10^{10}$ sec⁻¹ $> \omega_H$. These inequalities resulted in the validity of the general relations given above. The measured frequencies of the scattered radiation are in good agreement with those calculated from Eq. (1.2) (see Fig. 1). The electron beam from the Terek-1 accelerator has an energy spread⁶ $\Delta \varepsilon / \varepsilon \leq 0.1$. Therefore even in the most unfavorable case of scattering strictly backward, when $k_{0z} \approx k_0 \sim 2\omega_1'/c$, we have $\xi \leq 0.1$ and the condition for development of hydrodynamical instability⁷ (1.6) is satisfied for $P_1 \geq 20$ MW. This is in good agreement with the minimum threshold (of the order 10 MW) for observation of scattered radiation at a wavelength $\lambda_2 = 13.4 \pm 1$ mm. At the same time it should be noted that up to $P_1 \approx 300$ MW in our experiments only the resonance breakup instability could appear, since even in the most unfavorable case of scattering strictly backward we have $v_{E1}/c = v_E/c \ll (\omega_b/2\gamma\omega_1)^{1/2} \approx \frac{1}{3}$. Therefore we are justified in assuming that the spatial amplification coefficient of the scattered wave is $\Gamma \sim P_1^{1/2}$ [see Eqs. (1.4) and (1.5)].

The process of stimulated scattering by the beam can be written in the form

$$dP_2/dz = \beta_1 P_1 + \Gamma P_2, \quad (3.1)$$

where $\beta_1 = n_0 \sigma_T(\omega_2) \omega_2 / \omega_1$ characterizes the spontaneous Thomson scattering by the beam electrons with a frequency conversion $\omega_1 \rightarrow \omega_2$. Obviously $\sigma_T(\omega_2) \approx (e^2/mc^2)^2 = 10^{-25}$ cm². The second term in Eq. (3.1) characterizes the amplification of the scattered wave. Solution of Eq. (3.1) for a specified value $P_2(0) = P_0$ for $z = 0$ (for example, for the initial noise level in a given frequency range at the input to the system) leads to the following value of the scattered-radiation power at the output of the system:

$$P_2(L) = P_0 e^{\Gamma L} + \beta_1 P_1 \Gamma^{-1} (e^{\Gamma L} - 1). \quad (3.2)$$

If the radiation at frequency ω_2 leaves the system without reflection, the value of the power $P_2(L)$ of the departing scattered radiation is determined entirely by the single-traversal amplification (self-amplification). However, if a partial reflection occurs from the ends of the system with a reflection coefficient $\kappa(\omega_2)$, then multiple amplification of the scattered radiation is possible and for the power of the radiation leaving the system in the stationary regime [i. e., for $\kappa P_2(L) = P_0$] we have

$$P_2 = (1 - \kappa) \left(\frac{\kappa}{1 - \kappa e^{\Gamma L}} + 1 \right) \frac{\beta_1 P_1}{\Gamma} (e^{\Gamma L} - 1). \quad (3.3)$$

Hence it follows that for the condition

$$\kappa(\omega_2) e^{\Gamma L} \geq 1 \quad (3.4)$$

the power of the scattered radiation increases—the amplification of the scattering goes over into the generation mode.

It is evident from Eq. (3.2) that for $P_0 = 0$ (in the absence of noise in the system) and a low gain ($\Gamma L \ll 1$) we have $P_2 \approx \beta_1 P_1 L \lesssim 10^{-10} P_1$. Even for $P_1 \approx 300$ MW this gives $P_2 \lesssim 0.03$ W, which is significantly below the sensitivity of the receiving apparatus P_{min} (see the table). Therefore the very fact of observation of scattered radiation with a power above the sensitivity of the detecting equipment indicates a significant gain, i. e., $\Gamma L \gg 1$ in all scattered-radiation wavelength regions studied.

Assuming $\Gamma L \gg 1$, we have from Eq. (3.2)

$$P_2(L) = \left(P_0 + \frac{\beta_1 P_1 L}{\Gamma} \right) e^{\Gamma L}. \quad (3.5)$$

On the assumption that $P_2 \sim \exp(\alpha P_1^{1/2})$, we determined the value of the coefficient α from the experimental data shown in Fig. 3. It turned out that in the three scattered-radiation wavelength regions measured, the value of α is the same, amounting to $\alpha \approx 4.6 \times 10^{-4}$ W^{-1/2}. In evaluating α on the basis of Eq. (1.4) it is necessary to take into account the Lorentz transformations relating quantities in the beam coordinate system with the laboratory system, which are given in the Appendix. The results of this calculation for the indicated parameters of the system ($L = 60$ cm) in various frequency ranges are given in the table. It can be seen that the experimentally determined value of α corresponds qualitatively to the value calculated, which apparently indicates the resonance mechanism of breakup (Raman scattering). The experimentally determined value of α permits evaluation of the self-amplification coefficient, i. e., the quantity $e^{\Gamma L}$. Values of the self-gain in various frequency ranges are given in the table as a function of the power P_1 . In the wavelength range $\lambda_2 \leq 3.2$ mm for $P_1 = 300$ MW, we have $\beta_1 P_1 / \Gamma \approx 2.5 \times 10^{-3}$, $e^{\Gamma L} \approx 3 \times 10^3$, and as follows from Eq. (3.5), for $P_0 = 0$, $P_2 \approx 7.5$ W. This quantity of scattered radiation is in good agreement with the experimentally measured value $P_2 \approx 20$ W.

The quantity P_0 characterizing the initial noise level can be determined by fitting the experimental data shown in Fig. 3 by a function of the form $P_2 = P_0 \exp(\alpha P_1^{1/2})$. In this case P_0 is a normalizing factor. Values of P_0 for each frequency range are given in the table. In fitting the experimental data in the range $\lambda_2 = 13.5 \pm 1$ mm two normalization factors are necessary: $P_0 = 1000$ W (Fig. 3a, curve 1) and $P_0 = 1800$ W (Fig. 3a, curve 2). As can be seen from Fig. 3, a dependence of the form $P_2 = P_0 \exp(\alpha P_1^{1/2})$ satisfactorily fits the experimental data (solid curves). In the two shortest-wavelength frequency regions $P_0 < P_{min}$, and consequently this noise radiation could not be observed. In the wavelength region $\lambda_2 = 13.4 \pm 1$ mm we have $P_0 > P_{min}$. However, no noise radiation of this type was recorded in this frequency range. But if $P_0 \leq P_{min}$ under the conditions of the experiment, then the observed ratio $P_{2max} / P_{min} \approx 130$ kW/0.5 kW = 260 cannot be explained by the existence of a single self-gain $e^{\Gamma L} \approx 60$. It should be noted that the constriction 8 in Fig. 2, which is beyond

cutoff for the pumping wave, is also beyond cutoff for the scattered wave $\lambda_2 = 13.4$ mm (a diameter 20 mm, $\mu = 6.35$). Therefore a small reflection coefficient at the other end of the waveguide ($\kappa \approx 0.02$) is sufficient for the condition (3.4) to begin to be satisfied with increase of the power P_1 , i.e., with increase of Γ , and for additional amplification of the scattered-radiation power to occur. This is indicated also by the fact that in this frequency range $P_0 = P_0(P_1)$.

Thus, the entire set of experimental data indicates that in the situation investigated resonance breakup (Raman scattering) occurs. In the wavelength range $\lambda_2 \leq 3.2$ mm there is apparently a self-gain of spontaneous radiation or of noise radiation comparable to it in magnitude. In the wavelength regions 7.8 ± 0.5 and 4.75 ± 1.5 mm a self-gain of the noise radiation can occur. In the wavelength region 13.4 ± 1 mm for $P_1 = 10$ – 40 MW self-amplification of noise radiation also occurs, which on increase of the power P_1 with $P_1 > 60$ MW apparently goes over to the process of generation of the scattered radiation (curves 1 and 2, Fig. 3a).

The authors are grateful to S. I. Kremontsov, M. I. Petelin, and A. V. Smorgonskiĭ for helpful discussions and to L. É. Tsopp for making possible the use in this work of cryogenically cooled semi-conductor microwave detectors.

APPENDIX

Here we give a number of formulas of the Lorentz transformations relating quantities in the beam coordinate system and the laboratory system and making clear the relations given in §1:

$$\omega_1' = \gamma \omega_1 (1 + \beta \beta_{\text{lim}1}), \quad \omega_2' = \gamma \omega_2 (1 - \beta \beta_{\text{lim}2}),$$

$$\delta' = \gamma \delta (1 + \beta \beta_{\text{lim}2}), \quad k_{1\alpha}' = k_{1\alpha} = \mu_{\alpha 1} / R,$$

$$k_{z1}' = -\gamma \frac{\omega_1}{c} (\beta + \beta_{\text{lim}1}), \quad k_{z2}' = \gamma \frac{\omega_2}{c} (\beta_{\text{lim}2} - \beta),$$

$$\mathbf{k}_0 = \mathbf{k}_1' - \mathbf{k}_2' = (k_{1x}' - k_{2x}'; k_{1y}' - k_{2y}'),$$

$$\mathbf{E}_1' = (E_{1\perp 1}'; E_{1\parallel 1}') = \left(E_{1\perp 1} \frac{\omega_1'}{\omega_2} - \gamma \frac{\omega_{k1}}{\omega_1} E_{1\parallel 1}; E_{1\parallel 1} \right),$$

$$k_0 = \frac{1}{c} \{ (\omega_{k1} - \omega_{k2})^2 + \gamma^2 [\omega_1 (\beta + \beta_{\text{lim}1}) + \omega_2 (\beta_{\text{lim}2} - \beta)]^2 \}^{1/2},$$

$$[\mathbf{k}_2' \mathbf{v}_{x1}']^2 = k_{z2}'^2 v_{x1}'^2 \sin^2 \psi,$$

$$v_{x1}'^2 = \frac{e^2 E_1'^2}{m^2 \omega_1'^2} = \frac{e^2}{m^2 \omega_1'^2 \omega_1'^2} [\omega_1'^2 E_{1\parallel 1}'^2 + (\omega_1' E_{1\perp 1}' - \gamma \omega_{k1} \beta E_{1\parallel 1}')^2],$$

$$(\mathbf{k}_2' \mathbf{E}_1') = k_{z2}' E_1' \cos \psi = -\gamma \frac{\omega_2}{c} (\beta_{\text{lim}2} - \beta) E_{1\parallel 1}' + \frac{\omega_{k2}}{c} \left(\frac{\omega_1'}{\omega_1} E_{1\perp 1}' - \gamma \frac{\omega_{k1}}{\omega_1} \beta E_{1\parallel 1}' \right).$$

- ¹⁾ In reality, depending on the direction of \mathbf{k}_0 the quantity ω_0 varies within the limits from ω_b (for $\mathbf{k}_0 \parallel \mathbf{H}_0$ or $\omega_b^2 \gg \omega_{H0}^2$) to $\omega_0 = \omega_b k_{0x} / k_0$ for $\omega_b^2 \gg \omega_b^2$ (see for example Ref. 7).
²⁾ The kinetic instability has such a small increment that it could hardly appear in our experiments.

- ¹P. Dirac and P. L. Kapitza, Proc. Camb. Phys. Soc. **29**, 297 (1933).
²P. Sprangle and V. L. Granatstein, Appl. Phys. Lett. **25**, 377 (1974); P. Sprangle, V. L. Granatstein, and L. Baker, Phys. Rev. **A12**, 1697 (1975); IEEE-MTT **25**, 245 (1977). P. Sprangle, A. T. Drobot, NRL Report No. 3587, 1978.
³V. I. Miroshnichenko, Pis'ma Zh. Tekh. Fiz. **1**, 1057 (1975) [Sov. Tech. Phys. Lett. **1**, 453 (1975)]. Fiz. Plazmy **2**, 789 (1976) [Sov. J. Plasma Phys. **2**, 439 (1976)].
⁴N. Ya. Katsarenko and G. L. Fal'ko, Radiotekh. Élektron. **20**, 2519 (1975) [Radio Eng. Electron. (USSR)]; Pis'ma Tekh. Fiz. **4**, 189 (1978) [Sov. Tech. Phys. Lett. **4**, 000 (1978)].
⁵N. S. Bratman, N. S. Ginzburg, and M. I. Petelin, Pis'ma Zh. Eksp. Teor. Fiz. **28**, 207 (1978) [JETP Lett. **28**, 190 (1978)].
⁶G. P. Mkheidze and M. D. Raizer, Kratk. Soobshch. Fiz., FIAN SSSR, No. 4, 41 (1972).
⁷V. L. Ginzburg and A. A. Rukhadze, Volny v magnitoaktivnoi plazme (Waves in a Magnetoactive Plasma), Nauka, 1975.
⁸V. P. Silin, Parametricheskoe vozdeĭstvie izlucheniya bol'shoĭ moshchnosti na plazmu (Parametric Action of High-Power Radiation on Plasma), Nauka, 1973.
⁹N. E. Andreev, Zh. Eksp. Teor. Fiz. **59**, 2105 (1970) [Sov. Phys. JETP **32**, 1141 (1971)].
¹⁰N. F. Kovalev, M. I. Petelin, M. D. Raizer, A. V. Smorgonskiĭ, and L. É. Tsopp, Pis'ma Zh. Eksp. Teor. Fiz. **18**, 232 (1973) [JETP Lett. **18**, 138 (1973)].
¹¹M. D. Raizer and L. É. Tsopp, Radiotekh. Élektron. **8**, 1691 (1975) [Radio Eng. Electron. (USSR)].

Translated by Clark S. Robinson